$P2Y_2$ and G_q/G_{11} control blood pressure by mediating endothelial mechanotransduction

ShengPeng Wang,[1] András Iring,[1,2] Boris Strilic,[1] Julián Albarrán Juárez,[1] Harmandeep Kaur,[1] Kerstin Troidl,[1,3] Sarah Tonack,[1] Joachim C. Burbiel,[4] Christa E. Müller,[4] Ingrid Fleming,[5] Jon O. Lundberg,[6] Nina Wettschureck,[1,7] and Stefan Offermanns[1,7]

[1]Max Planck Institute for Heart and Lung Research, Department of Pharmacology, Bad Nauheim, Germany. [2]Institute of Human Physiology and Clinical Experimental Research, Semmelweis University, Budapest, Hungary. [3]Department of Vascular and Endovascular Surgery, University Hospital Frankfurt, Frankfurt am Main, Germany. [4]PharmaCenter Bonn, Pharmaceutical Institute, Pharmaceutical Chemistry I, University of Bonn, Bonn, Germany. [5]Institute for Vascular Signalling, Centre for Molecular Medicine, Goethe-University, Frankfurt am Main, Germany. [6]Department of Physiology and Pharmacology, Karolinska Institutet, Stockholm, Sweden. [7]Centre for Molecular Medicine, University of Frankfurt, Frankfurt am Main, Germany.

Elevated blood pressure is a key risk factor for developing cardiovascular diseases. Blood pressure is largely determined by vasodilatory mediators, such as nitric oxide (NO), that are released from the endothelium in response to fluid shear stress exerted by the flowing blood. Previous work has identified several mechanotransduction signaling processes that are involved in fluid shear stress–induced endothelial effects, but how fluid shear stress initiates the response is poorly understood. Here, we evaluated human and bovine endothelial cells and found that the purinergic receptor $P2Y_2$ and the G proteins G_q/G_{11} mediate fluid shear stress–induced endothelial responses, including $[Ca^{2+}]_i$ transients, activation of the endothelial NO synthase (eNOS), phosphorylation of PECAM-1 and VEGFR-2, as well as activation of SRC and AKT. In response to fluid shear stress, endothelial cells released ATP, which activates the purinergic $P2Y_2$ receptor. Mice with induced endothelium-specific $P2Y_2$ or G_q/G_{11} deficiency lacked flow-induced vasodilation and developed hypertension that was accompanied by reduced eNOS activation. Together, our data identify $P2Y_2$ and G_q/G_{11} as a critical endothelial mechanosignaling pathway that is upstream of previously described mechanotransduction processes and demonstrate that $P2Y_2$ and G_q/G_{11} are required for basal endothelial NO formation, vascular tone, and blood pressure.

Introduction

Hypertension is a primary risk factor for cardiovascular diseases including myocardial infarction and stroke (1, 2). Vascular tone and blood pressure are controlled under physiological and pathophysiological conditions by various autoregulatory functions of blood vessels. One of the fundamental autoregulatory processes that adapts vessel diameter to blood flow and critically contributes to vascular tone and blood pressure is the flow-induced relaxation of vascular smooth muscle (3). In response to fluid shear stress, the vascular endothelium releases a variety of vasoactive factors (4, 5). Of these, nitric oxide (NO) produced by endothelial NO synthase (eNOS or NOS3) plays a predominant role in flow-induced vasodilation (6). Acute flow induces a transient increase in $[Ca^{2+}]_i$, which leads to Ca^{2+}/calmodulin-dependent eNOS activation. However, the maintained activation of NO formation in response to shear stress requires phosphorylation of eNOS at serine 1177 by AKT kinases (7, 8) or other protein kinases, such as protein kinase A (PKA) (6, 9). The adhesion molecule PECAM-1 has been implicated in the shear stress–induced activation of AKT kinases and eNOS as well as in flow-mediated vasodilation (10–12), but it can also mediate inflammatory signaling in response to disturbed flow (13–15). PECAM-1 forms a complex with vascular endothelial cadherin (VE-cadherin), which, following the shear stress–induced tyrosine phosphorylation of PECAM-1, recruits VEGFR-2. VEGFR-2 in turn becomes tyrosine phosphorylated and activates downstream signaling events including the activation of AKT kinases (13, 16). Biophysical evidence indicated that PECAM-1 is not a primary mechanosensor, but that it is controlled by upstream mechanisms that have remained elusive (17, 18). Other mechanotransducers suggested to date include mechanosensitive ion channels (19–21), the endothelial glycocalyx layer (22, 23), and the primary cilium (24). Also, pertussis toxin–sensitive and –insensitive heterotrimeric G proteins have been linked with fluid shear stress–induced endothelial signaling (25–28), and the G proteins G_q and G_{11} have recently been shown to interact with PECAM-1 and to mediate fluid shear stress–induced AKT phosphorylation (27, 28). Thus, previous work has identified several mechanotransduction signaling processes involved in fluid shear stress–induced endothelial effects (29, 30); however, these mechanotransduction processes have primarily been studied in vitro using isolated endothelial cells, and their in vivo role as well as the upstream regulatory mechanisms are unclear.

Here, we show that the endothelial $P2Y_2$ receptor, coupled to the G proteins G_q and G_{11}, plays a critical role in fluid shear stress–induced eNOS activation and thereby controls vascular tone and blood pressure.

Results

G_q/G_{11} mediate endothelial response to fluid shear stress in vitro. To test the role of the heterotrimeric G proteins G_q and G_{11} in fluid

Conflict of interest: The authors have declared that no conflict of interest exists.
Submitted: January 20, 2015; **Accepted:** May 28, 2015.
Reference information: *J Clin Invest*. 2015;125(8):3077–3086. doi:10.1172/JCI81067.

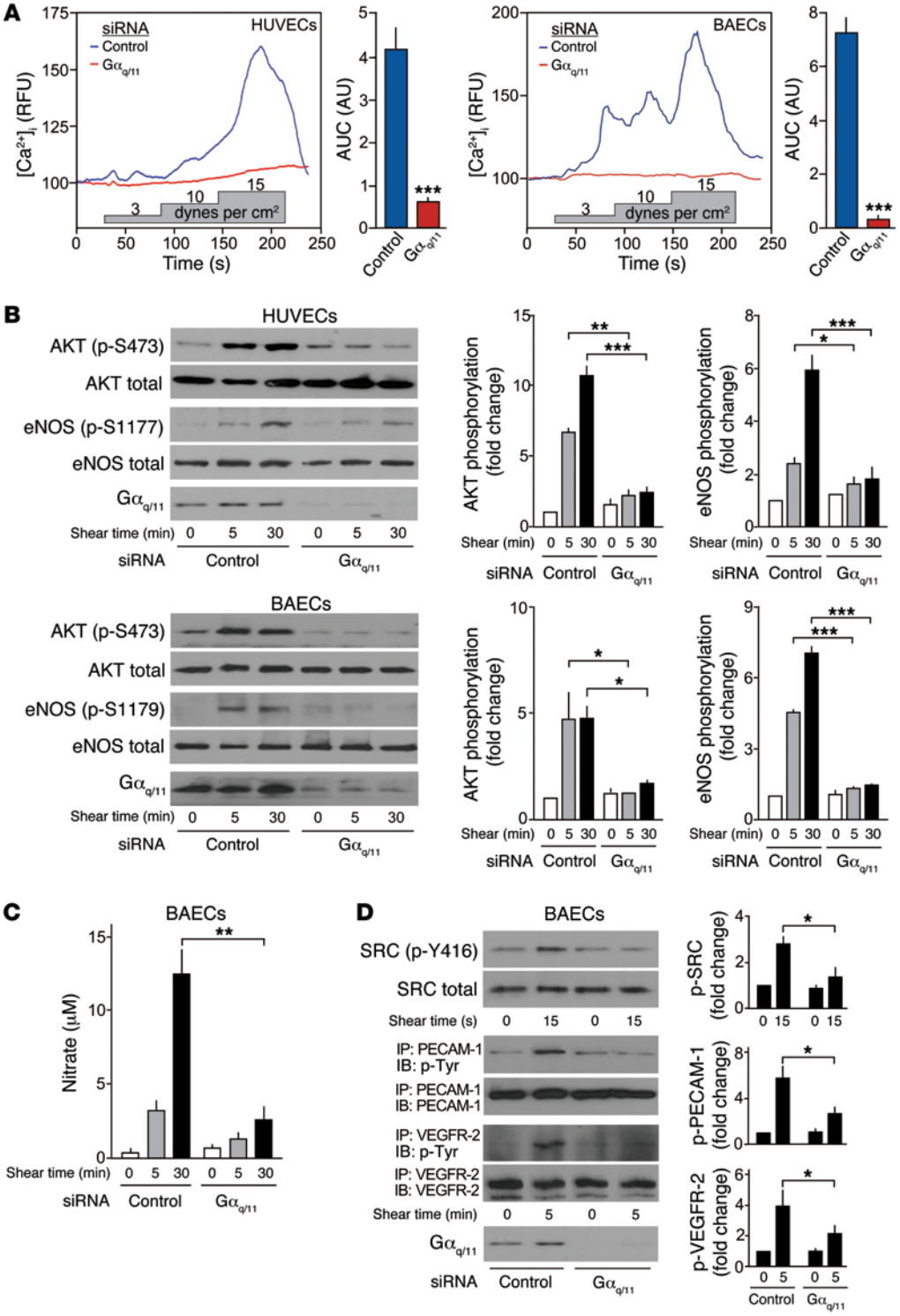

Figure 1. G_q and G_{11} mediate endothelial response to fluid shear stress in vitro. The indicated cells were transfected with scrambled (control) siRNA, or an siRNA directed against $G\alpha_q$ and $G\alpha_{11}$. (**A**) Fluo-4–loaded HUVECs (n = 21, control; n = 25, $G\alpha_{q/11}$; 3 independent experiments) and BAECs (n = 23, control; n = 16, $G\alpha_{q/11}$; 3 independent experiments) were exposed to the indicated shear forces, and $[Ca^{2+}]_i$ was determined as fluorescence intensity (RFU, relative fluorescence units). Graphs show the AUC. Data represent the mean ± SEM; $^{***}P \le 0.001$, by 2-tailed Student's t test. (**B**–**D**) HUVECs and BAECs (n = 3) were exposed to fluid shear (12 and 20 dynes/cm^2, respectively) for the indicated durations. AKT, eNOS, and SRC activation (**B** and **D**) was determined by Western blotting for phosphorylated AKT, eNOS, and SRC kinases and total AKT, eNOS, and SRC. PECAM-1 and VEGFR-2 activation (**D**) was determined by IP and Western blotting for tyrosine phosphorylated PECAM-1 and VEGFR-2 . Knockdown of $G\alpha_q/G\alpha_{11}$ was verified by anti-$G\alpha_q/G\alpha_{11}$ immunoblotting. Graphs show the densitometric evaluation. **C**, Nitrate concentration in the cell medium. Data represent the mean ± SEM; $^{*}P \le 0.05$, $^{**}P \le 0.01$, and $^{***}P \le 0.001$, by 2-way ANOVA, with Bonferroni's post-hoc test. p, phosphorylated; S, serine.

shear stress–induced endothelial responses, we determined the effect of siRNA-mediated knockdown of the α subunits of G_q and G_{11}, $G\alpha_q$ and $G\alpha_{11}$, on shear stress–induced cellular effects in HUVECs and bovine aortic endothelial cells (BAECs). Suppression of $G\alpha_q/G\alpha_{11}$ expression strongly reduced shear stress–induced increases in $[Ca^{2+}]_i$ (Figure 1A). It also reduced thrombin-induced effects, but had no effect on ionomycin-induced increases in $[Ca^{2+}]_i$ (Supplemental Figure 1, A and B). Similarly, knockdown of $G\alpha_q/G\alpha_{11}$ strongly reduced phosphorylation of AKT (at serine 473) and eNOS (at serine 1177 and serine 1179) induced by laminar flow in HUVECs and BAECs, respectively (Figure 1B). The same result was found after an acute increase in flow (Supplemental Figure 1C). Also, the effect of carbachol, which activates G_q/G_{11}-coupled muscarinic receptors, on eNOS and AKT phosphorylation was prevented after knockdown of $G\alpha_q/G\alpha_{11}$ expression. However, the effect of insulin, which acts independently of G_q/G_{11}, was unaffected (Supplemental Figure 1D), indicating that the cells had not lost the ability to respond to all stimuli. Loss of flow-induced effects

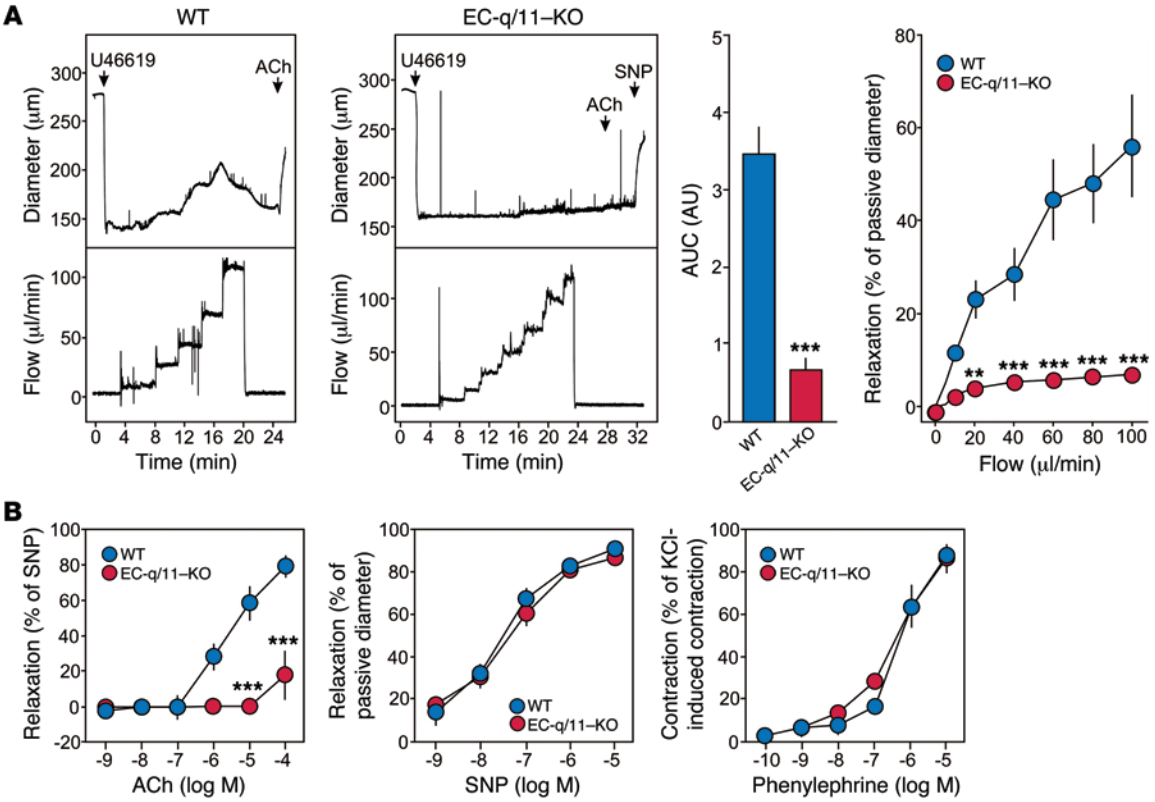

Figure 2. Endothelial $G\alpha_q$ and $G\alpha_{11}$ are required for flow-induced vasodilation. (**A** and **B**) Mesenteric arteries from tamoxifen-treated WT or EC-q/11–KO mice were exposed to flow and various agents. (**A**) Effect of a stepwise increase in perfusion flow on the diameter of vessels precontracted with 100 nM of the thromboxane A_2 analog U46619. After flow was stopped, 10 μM ACh and 100 μM SNP were added. Shown is the evaluation of the AUC and the time course of flow-induced vasorelaxation as a percentage of the passive vessel diameter (n = 6, WT; n = 8, EC-q/11–KO). (**B**) Effect of ACh, SNP, and phenylephrine on vascular diameter (n = 6). Data represent the mean ± SEM; $^{**}P \leq 0.01$ and $^{***}P \leq 0.001$, by 2-tailed Student's t test (**A**, middle) and 2-way ANOVA, with Bonferroni's post-hoc test (**A**, right and **B**).

after knockdown of $G\alpha_q$ and $G\alpha_{11}$ was verified by using at least one additional siRNA (data not shown), and knockdown of $G\alpha_q/G\alpha_{11}$ expression had no effect on the expression of various other genes encoding proteins involved in cellular signaling or flow sensing (Supplemental Figure 1F). The reduced flow-induced eNOS phosphorylation after knockdown of $G\alpha_q/G\alpha_{11}$ expression was accompanied by a loss of the flow-induced increases in nitrate levels in cell supernatants (Figure 1C), indicating reduced eNOS activity. Consistent with a role of SRC and VEGFR-2 in flow-induced phosphorylation of eNOS and AKT, blockade of SRC and VEGFR-2 kinase activity with PP2 and Ki8751, respectively, abrogated both effects (Supplemental Figure 1E). The fluid shear stress–induced tyrosine phosphorylation of SRC kinases PECAM-1 and VEGFR-2 were also markedly reduced after knockdown of $G\alpha_q/G\alpha_{11}$ (Figure 1D), demonstrating that G_q and G_{11} operate upstream of these signaling molecules in sensing fluid shear stress.

Endothelial G_q/G_{11} deficiency results in loss of flow-induced vasodilation and hypertension. To test the physiological relevance of G_q/G_{11} in endothelial flow sensing, we determined the flow-induced vasodilation of murine mesenteric arteries. In precontracted vessels isolated from inducible endothelium-specific $G\alpha_q/G\alpha_{11}$-deficient mice (*Tie2-CreER^{T2} Gnaq$^{fl/fl}$ Gna11$^{-/-}$*, herein referred to as EC-q/11–KO) (31), dilation in response to flow was almost completely lost (Figure 2A). Also, acetylcholine-induced (ACh-induced) vasodilation, which is mediated by the G_q/G_{11}-coupled muscarinic M3 receptor (32), was strongly inhibited (Figure 2B). However, vessels from EC-q/11–KO mice were fully responsive to the endothelium-independent vasodilator sodium nitroprusside (SNP) and the vasoconstrictor phenylephrine (Figure 2B), indicating that contractile and vasodilatory functions, per se, were not affected.

Flow-induced vasodilation is regarded as a basic mechanism critically contributing to vascular tone and basal blood pressure (29). While treatment of WT mice with tamoxifen had only a small, transient effect on mean arterial blood pressure, the induction of endothelial $G\alpha_q/G\alpha_{11}$ deficiency in EC-q/11–KO mice by tamoxifen (31) resulted in a significant increase of approximately 20 mmHg within a few days (Figure 3A). The development of hypertension was paralleled by a decrease in plasma nitrate levels (Figure 3B) as well as by the attenuated phosphorylation of the murine mesenteric artery eNOS at serine 1176 (Figure 3C). This indicates that acute loss of endothelial G_q/G_{11}-mediated signaling strongly reduces eNOS activity in vivo, resulting in reduced NO formation, increased vascular tone, and arterial hypertension.

As shown previously, the ligation of the external carotid artery results within 2 weeks in a reduced diameter of the common carotid artery (33, 34). This process is believed to depend on endothelial flow sensing and is strongly inhibited in mice lacking eNOS (33). Consistent with an eNOS-mediated role of endothelial G_q/G_{11}

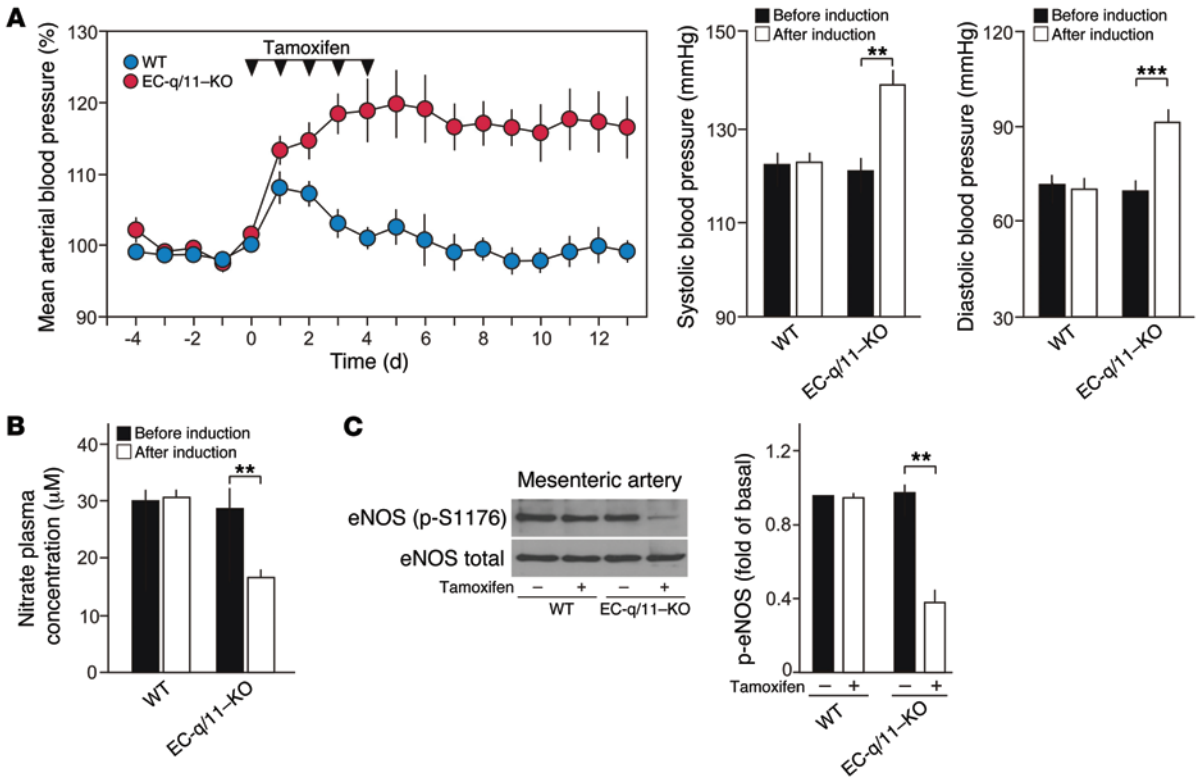

Figure 3. Induction of endothelial G_q/G_{11} deficiency results in reduced eNOS activation and hypertension. (**A**) Telemetrically recorded blood pressure in WT (n = 9) and EC-q/11–KO (n = 8) mice before, during, and after administration of tamoxifen for 5 days. Average blood pressure 5 days before induction was set to 100%. Graphs show systolic and diastolic arterial blood pressure 4 days before tamoxifen treatment and in the second week after induction. (**B**) Plasma nitrate levels in WT (n = 12) and EC-q/11–KO mice (n = 12) before and 10 days after induction. (**C**) Phosphorylation of eNOS at serine 1176 in lysates from mesenteric arteries prepared before (–) or 3 days after (+) tamoxifen induction in WT and EC-q/11–KO. Graph shows the densitometric evaluation (n = 4). Data represent the mean ± SEM; $^{**}P \leq 0.01$ and $^{***}P \leq 0.001$, by 2-tailed Student's t test.

in flow-mediated remodeling, we found that the diameter of the common carotid artery did not significantly change in response to ligation of the external carotid artery in EC-q/11–KO mice compared with WT animals (Supplemental Figure 2A). EC-q/11–KO mice also showed a strong reduction in neointima formation after ligation of the common carotid artery (Supplemental Figure 2B). These data indicate that endothelial G_q/G_{11}-mediated signaling is also required for flow-mediated vascular remodeling.

$P2Y_2$ mediates endothelial fluid shear stress response and controls vascular tone and blood pressure. To identify potential GPCRs operating upstream of G_q/G_{11}, we analyzed the expression of GPCRs in HUVECs and human umbilical artery endothelial cells (HUAECs) and performed an siRNA-mediated knockdown of 42 receptors expressed in both cell types (Supplemental Figure 3, A and B). Knockdown of the purinergic $P2Y_2$ receptor had by far the strongest effect on fluid shear stress–induced AKT phosphorylation in HUVECs (Supplemental Figure 3, B and C). $P2Y_2$ is a G_q/G_{11}-coupled receptor activated by ATP and uridine triphosphate (UTP) (35), and an alternative siRNA directed against $P2Y_2$ was able to almost completely abrogate flow-induced Ca^{2+} transients (Figure 4A) as well as Ca^{2+} transients induced by the $P2Y_2$ agonists ATP and UTP (Supplemental Figure 4A). Also, flow-induced AKT and eNOS phosphorylation, as well as tyrosine phosphorylation of SRC kinase, PECAM-1, and VEGFR-2, were strongly reduced by the knockdown of $P2Y_2$ (Figure 4B). Similarly, the $P2Y_2$ receptor antagonist AR-C118925 blocked fluid shear stress–induced AKT and eNOS phosphorylation (Figure 4C), whereas knockdown of the main endothelial ionotropic purinergic receptor P2X4 had no effect (Supplemental Figure 4B). Knockdown of $P2Y_2$ also strongly reduced shear stress–induced increases in nitrate levels in cell supernatants (Figure 4D) and blocked ATP-induced, but not insulin-induced, AKT and eNOS phosphorylation (Supplemental Figure 4C). The expression of various genes encoding proteins involved in cellular signaling or flow sensing was not affected by knockdown of $P2Y_2$ (Supplemental Figure 4D). Consistent with previous data (36–39), we found that fluid shear stress induced the release of considerable amounts of ATP from endothelial cells (Figure 4E). Interestingly, flow- but not insulin-induced AKT and eNOS phosphorylation was strongly reduced when ATP in the medium was degraded by apyrase (Figure 4, F and G), and apyrase also inhibited flow-induced NO formation (Figure 4H).

We then generated inducible endothelium-specific $P2Y_2$-deficient mice (*Tie2-CreER^{T2} P2ry2$^{fl/fl}$*, herein referred to as EC-$P2Y_2$–KO mice; Supplemental Figure 5) to investigate the physiological role of $P2Y_2$ in fluid shear stress–induced eNOS activation and found that precontracted mesenteric arteries from EC-$P2Y_2$–KO mice no longer responded to increases in flow with vasodilatation but showed normal responses to the NO donator sodium nitroprusside and to the $P2Y_2$-independent vasodilator ACh (Figure 5A). Induction of endothelium-specific $P2Y_2$ deficiency in vivo

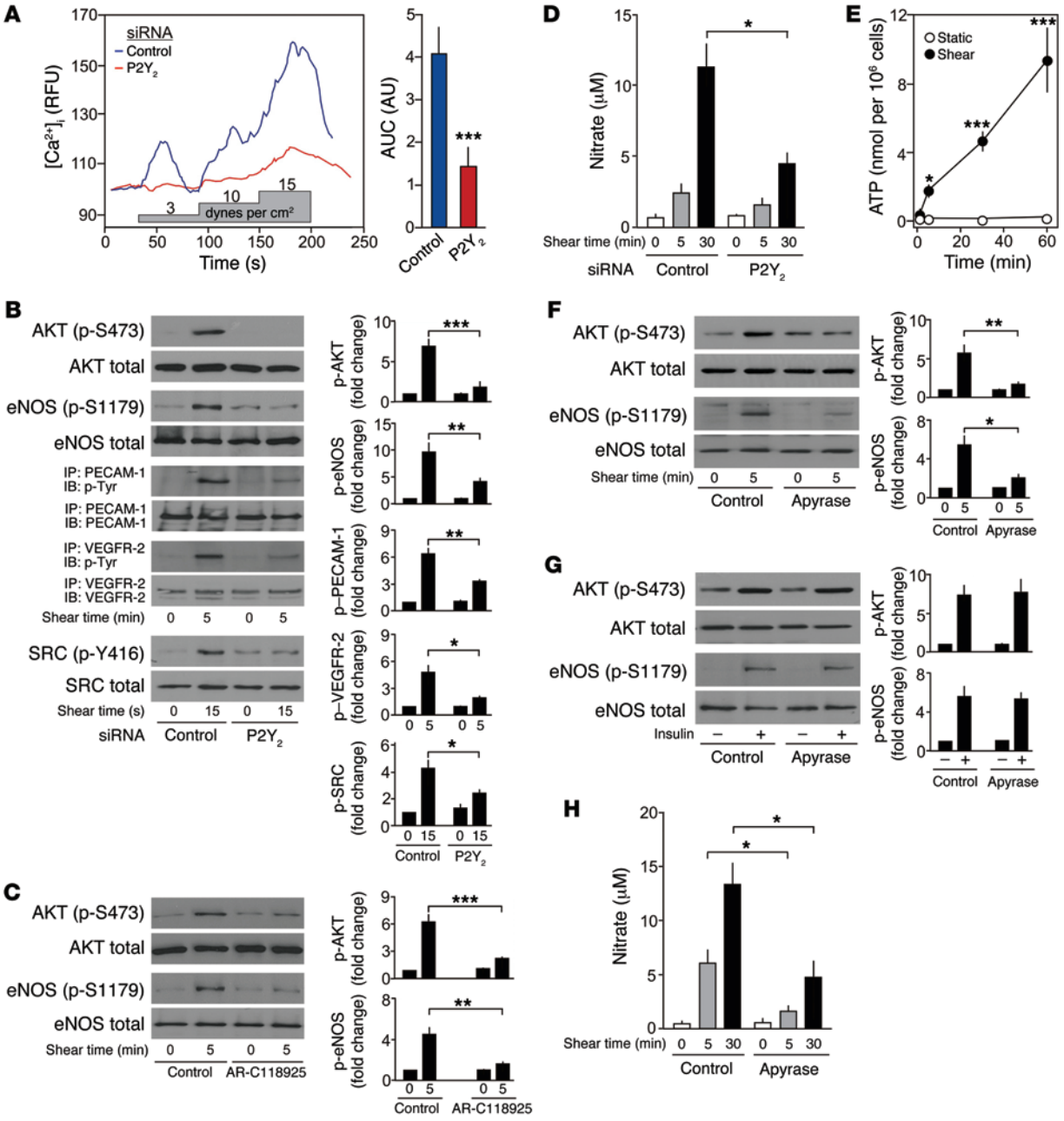

Figure 4. $P2Y_2$ mediates endothelial fluid shear stress response in vitro. (**A**–**D**) BAECs were transfected with scrambled siRNA (control) or siRNA directed against $P2Y_2$ (**A**, **B**, and **D**) or were preincubated without or with 30 μM of the $P2Y_2$ antagonist AR-C118925 (**C**). In the Fluo-4–loaded cells (**A**; n = 28 [control], n = 18 [$P2Y_2$]; 3 independent experiments), the effect of the indicated shear forces on $[Ca^{2+}]_i$ was determined as AUC and RFU fluorescence intensity. In **B** and **C**, cells were exposed to fluid shear (20 dynes/cm^2) for the indicated durations, and AKT, eNOS, SRC, PECAM-1, and VEGFR-2 activation was determined as described. Graphs show the densitometric evaluation (n = 3). (**D**) Nitrate concentration in the cell medium (n = 3). (**E**) Amount of ATP in the supernatant of BAECs kept under static conditions or under flow (20 dynes/m^2) for the indicated durations (n = 4). (**F**–**H**) BAECs (n = 4) were exposed to fluid shear (**F** and **H**; 20 dynes/cm^2) or to 1 μM insulin for 10 minutes (**G**) in the absence or presence of 10 U/ml apyrase. AKT and eNOS activation was determined by Western blotting for phosphorylated and total AKT and eNOS (**F** and **G**). Bar diagrams show the densitometric evaluation. (**H**) Nitrate concentration in the cell medium. Data represent the mean ± SEM; *$P \le 0.05$, **$P \le 0.01$, and ***$P \le 0.001$, by 2-tailed Student's t test (**A**) and 2-way ANOVA, with Bonferroni's post-hoc test (**B**–**H**).

recapitulated the phenotype of induced endothelial $G\alpha_q/G\alpha_{11}$ deficiency and resulted in a 20 mmHg increase in arterial blood pressure (Figure 5B), accompanied by attenuated eNOS phosphorylation (Figure 5C), strongly indicating $P2Y_2$ as the upstream regulator of G_q/G_{11} in fluid shear stress–dependent regulation of NO formation, vascular tone, and blood pressure.

Discussion

Under the influence of fluid shear stress exerted by flowing blood, the endothelium releases vasodilatory factors such as NO, which are important determinants of blood pressure under normal conditions as well as in hypertension. Previous work has identified several mechanotransduction signaling processes involved in

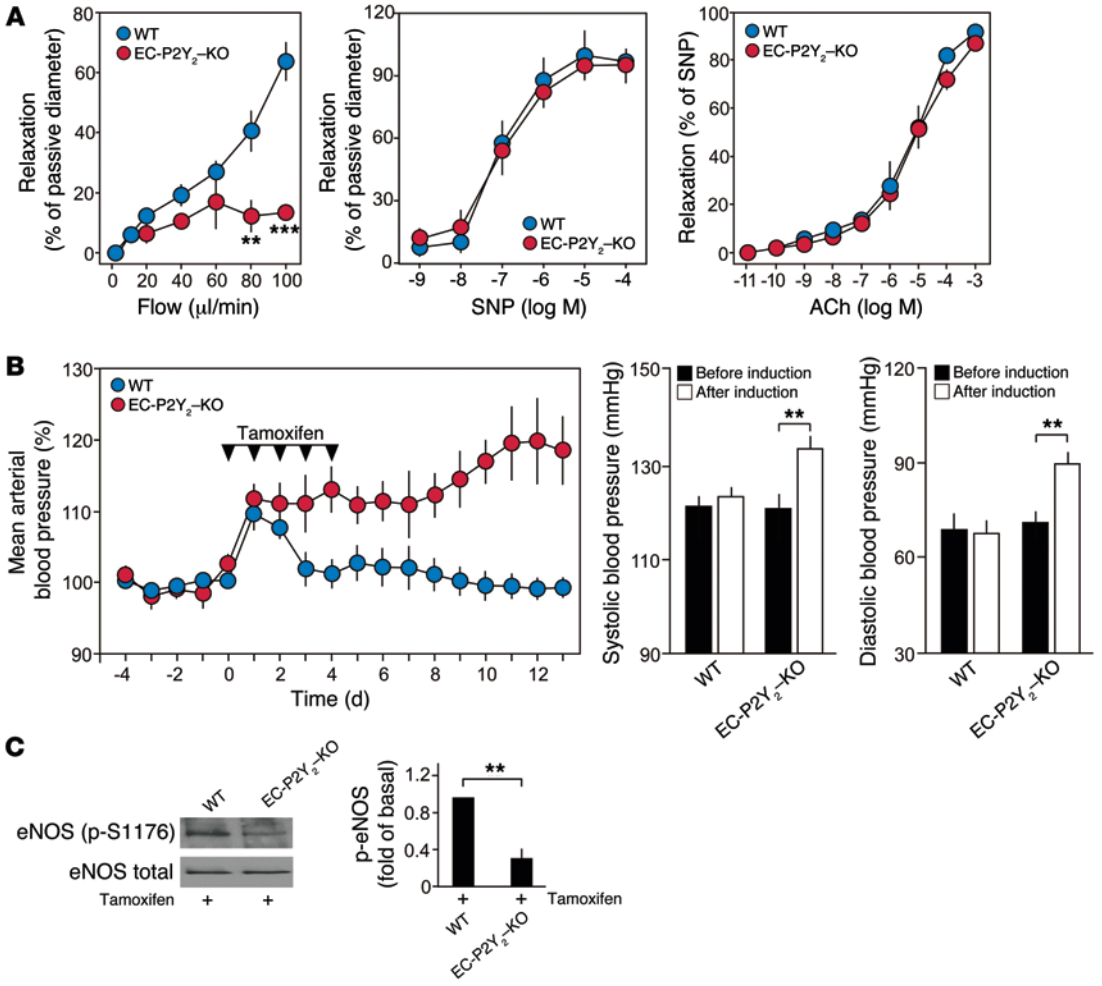

Figure 5. Endothelial $P2Y_2$ controls vascular tone and blood pressure. (**A**) Effect of increased perfusion flow (left) and increasing SNP (middle) and ACh concentrations (right) on the diameter of mesenteric arteries from WT (left: $n = 9$; middle: $n = 3$; right: $n = 6$) and EC-$P2Y_2$–KO (left: $n = 13$; middle: $n = 3$; right: $n = 6$) mice. Vessels were precontracted with 100 nM U46619. (**B**) Blood pressure in WT ($n = 9$) and EC-$P2Y_2$–KO mice ($n = 8$) before, during, and after induction. Average blood pressure 5 days before induction was set to 100%. Graphs show systolic and diastolic arterial blood pressure 4 days before tamoxifen treatment and in the second week after induction. (**C**) Phosphorylation of eNOS at serine 1176 in lysates from mesenteric arteries prepared 3 days after induction in WT and EC-$P2Y_2$–KO mice. Graph shows a densitometric evaluation ($n = 4$). Data represent the mean ± SEM; $^*P \le 0.05$. $^{**}P \le 0.01$, and $^{***}P \le 0.001$, by 2-tailed Student's t test (**B** and **C**) and 2-way ANOVA, with Bonferroni's post-hoc test (**A**).

fluid shear stress–induced endothelial effects (29, 30), but how fluid shear stress initiates these responses is poorly understood. Here, we show that the endothelial $P2Y_2$ receptor and G_q/G_{11} are required to activate the mechanosensory complex consisting of PECAM-1, VE-cadherin, and VEGFR-2 in response to fluid shear stress, a process likely to involve SRC kinases, which are rapidly activated by fluid shear stress in a G_q/G_{11}-dependent manner. In contrast to independent studies (27, 28), we could not detect any direct interaction between $G\alpha_q/G\alpha_{11}$ and PECAM-1 (data not shown), and we found G_q/G_{11} to be acting upstream of PECAM-1. We also demonstrate that the $P2Y_2/G_q/G_{11}$-mediated pathway is responsible for flow-induced NO formation by eNOS and for maintaining basal blood pressure. Acute eNOS activation through $P2Y_2$ and G_q/G_{11} may involve a transient increase in $[Ca^{2+}]_i$ which leads to Ca^{2+}/calmodulin-dependent eNOS activation. However, sustained activation of NO formation in response to shear stress is likely to involve $P2Y_2$- and G_q/G_{11}-mediated AKT activation, which leads to phosphorylation of eNOS at serine 1177 (7, 8). The fact that acute loss of endothelial $P2Y_2$-G_q/G_{11}–mediated signaling strongly reduces eNOS activity in vivo, resulting in arterial hypertension, indicates that the $P2Y_2$- and G_q/G_{11}-mediated signaling pathway in endothelial cells is constantly activated to sustain endothelial NO formation and to mediate fluid shear stress–induced vasodilation. The degree of arterial hypertension after long-term loss of endothelial expression of $G\alpha_q/G\alpha_{11}$ is much smaller than after acute induction of endothelial $G\alpha_q/G\alpha_{11}$ deficiency (31), suggesting that local and systemic counterregulatory processes are induced by the acute reduction in flow-induced G_q/G_{11}-mediated vasorelaxation.

In recent years, several GPCRs have been shown to respond to different mechanical stimuli in vitro (40). Of those, the G_q/G_{11}-coupled bradykinin B2 receptor showed conformational changes in response to fluid shear stress, demonstrated by intramolecular Förster resonance energy transfer of the heterologously expressed receptor fused with 2 fluorescent proteins (41). However, it is not known whether this also occurs in the WT receptor and results in activation of downstream signaling. In our expression analysis,

we did not find the B2 receptor consistently expressed in fluid shear stress–sensitive endothelial cells. Also, the sphingosine 1 phosphate receptor 1 (S1P1), which is widely expressed in different endothelia, has been involved in fluid shear stress sensing in vitro and in vivo (42), but it is not known whether endothelial S1P1 regulates vascular tone and blood pressure. However, given that S1P1 is coupled to G_i-type G proteins (43) and thereby activates downstream signaling pathways other than $P2Y_2$, it is likely that S1P1 mediates different flow-induced endothelial effects, such as endothelial cell alignment (42). It is also possible that both receptors to some degree synergize in endothelial flow sensing.

Although, the $P2Y_2$- and G_q/G_{11}-mediated signaling pathway is upstream of the mechanotransducing pathways described thus far, the question remains of how $P2Y_2$ is activated in response to flow. Evidence has been provided that GPCRs such as the S1P1 and the bradykinin B2 receptors can be activated by flow in a ligand-independent manner (41, 42). On the other hand, it is well known that increased shear stress on endothelial cells induces the release of the $P2Y_2$ agonist ATP and that ATP can activate $P2Y_2$ in isolated endothelial cells (36–39). Consistent with this, we found that fluid shear stress induced the release of considerable amounts of ATP from endothelial cells, and the ATP-degrading enzyme apyrase has been shown to block flow-induced increases in intracellular [Ca^{2+}] (44). In addition, we found that flow-induced AKT and eNOS phosphorylation, in addition to NO formation, was strongly reduced in the presence of apyrase, indicating that ATP mediates fluid shear stress–induced effects. Thus, flow-induced endothelial release of ATP through as-yet poorly understood mechanisms (45) is the most likely flow-dependent activation mechanism of $P2Y_2$.

Also, ionotropic purinergic receptors have been involved in flow-dependent endothelial effects, and, in particular, P2X4 has been suggested to mediate ATP-induced Ca^{2+} influx in endothelial cells as well as flow-dependent control of vascular tone (34, 46). However, a more recent study indicated that ATP-induced Ca^{2+} mobilization and NO production in vitro involve $P2Y_2$ rather than P2X receptors (47), and it remains unclear whether the elevated blood pressure and defective adaptive vascular remodeling seen in a global, nonconditional knockout of the P2X4-encoding gene in mice can be attributed to the loss of P2X4 in endothelial cells or other cells (34).

The ability of the endothelium to sense fluid shear stress and to transmit this information into an intracellular signal is a fundamental function of the endothelial cell layer of blood vessels. Shear stress sensing and transduction control vascular tone and morphogenesis and affect susceptibility to diseases, such as atherosclerosis and hypertension. We have identified a critical mechanosensing pathway consisting of $P2Y_2$ and G_q/G_{11} that is required for flow-dependent NO formation and regulation of vascular tone in vitro and in vivo. This pathway appears to be upstream of all mechanotransducing pathways described so far, and it may be interesting to investigate its function in other responses of endothelial cells to fluid shear stress as well as in vascular diseases such as hypertension.

Methods

Reagents. ACh, ATP, UTP, ATPγS, thrombin, carbachol, ionomycin, phenylephrine, PP2, and tamoxifen were purchased from Sigma-Aldrich. Insulin was purchased from Gibco. SNP was obtained from Alexis Biochemicals. Apyrase was purchased from New England BioLabs Inc. (catalog M0393L). Ki8751 was obtained from Tocris. The $P2Y_2$ receptor antagonist AR-C118925 was synthesized in the laboratory of Christa E. Müller (University of Bonn, Bonn, Germany); the purity was approximately 95% (determined by HPLC-UV/MS and ^{1}H- and ^{13}C-NMR). U46619 was from Cayman Chemical. Antiphosphorylated eNOS (mouse S1176, human S1177, and bovine S1179; catalog 9571); antiphosphorylated ADT (S473; catalog 4060); anti-AKT (catalog 9272); anti-GAPDH (catalog 2118); and antiphosphorylated SRC kinase (Y416; catalog 2113) Abs were obtained from Cell Signaling Technology. Antiphosphorylated tyrosine Ab (4G10; catalog 05-1050X) was obtained from EMD Millipore. Anti-eNOS Ab was purchased from BD Biosciences (catalog 610296). Anti-$G\alpha_q/G\alpha_{11}$ (catalog sc-392); anti–PECAM-1 (catalog sc-1506); anti-SRC (catalog sc-18); and anti–VEGFR-2 (catalog sc-505) Abs were purchased from Santa Cruz Biotechnology Inc.

Primary cells. HUVECs, HUAECs, and BAECs were obtained from Lonza, cultured with endothelial growth medium (EGM-2; Lonza), and confluent cells at a passage of 4 or less were used in experiments.

siRNA-mediated knockdown. Cells were transfected with siRNAs using Opti-MEM and Lipofectamine RNAiMAX (Invitrogen) as described previously (48). SiRNAs used for the screen were pools of siRNAs of an siRNA library directed against 514 genes encoding GPCRs including 407 non-olfactory human GPCRs and 86 olfactory human GPCRs (QIAGEN) targeting the same RNA. siRNAs against $G\alpha_q$, $G\alpha_{11}$, $P2Y_2$, and P2X4 were from QIAGEN. The targeted sequences of siRNAs directed against RNAs encoding $G\alpha_q$, $G\alpha_{11}$, $P2Y_2$, and P2X4 were as follows: *GNAQ* (human) 5′-CAGGACACATCGTTCGATTTA-3′ and 5′-CAGGAATGCTATGATAGACGA-3′; *GNA11* (human) 5′-CTACAAGTACGAGCAGAACAA-3′ and 5′-AACGTGACATCCATCATGTTT-3′; *Gnaq* (bovine) 5′-CACCAAGCTGGTGTATCAGAA-3′ and 5′-AACAATTTGCATAATACTAAT-3′; *Gna11* (bovine) 5′-CCATGATGGCGTGTTGCCTGA-3′ and 5′-CACGTTCATCAAGCAGATGCG-3′; *P2RY2* (human) 5′-CCCTTCAGCACGGTGCTCT-3′, 5′-CTGCCTAGGGCCAAGCGCA-3′, and 5′-GCTCGTACGCTTTGCCCGA-3′; *P2ry2* (bovine) 5′-CAGTCCAAGGGATGCATGT-3′, 5′-CTGCACAGGTCCTACGGAA-3′, and 5′-CCCTTCAGCACCGTGCTCT-3′; *P2RX4* (human) 5′-GAATCTGATTGAGTCTCCA-3′; and *P2rx4* (bovine) 5′-CTCATCAAGGCCTATGGCA-3′.

Shear stress assays, Western blotting, IP. For biochemical experiments, cells were exposed to flow using a parallel-plate flow chamber from ibidi (ibidi GmbH). For IP experiments after flow, the BioTech-Flow System (MOS Technologies) was used to expose cells to fluid shear stress. Cells were lysed in Triton X-100 buffer supplemented with protease and phosphatase inhibitors. Isolated mesenteric arteries were lysed by radioimmunoprecipitation assay (RIPA) buffer. Soluble supernatants were incubated with appropriate Abs and protein A/G PLUS-Agarose (Santa Cruz Biotechnology Inc.) overnight at 4°C. The beads were washed 5 times with lysis buffer. IPs or total cell lysates were subjected to SDS-PAGE and transferred to nitrocellulose membranes. Membranes were probed with primary and horseradish peroxidase–conjugated secondary Abs (Cell Signaling Technology) and were developed using the ECL detection system (Thermo Scientific Pierce, Life Technologies).

Determination of $[Ca^{2+}]_i$. For the determination of intracellular Ca^{2+} concentration, cells were placed in a microfluidic plate (Flux-

ion Biosciences) and loaded with Fluo-4 AM (Molecular Probes, Life Technologies). Laminar shear stress was generated using the BioFlux 200 System (Fluxion Biosciences), and live cell images were acquired with an Olympus IX81 microscope.

Determination of ATP concentration. Cells were kept under static conditions or exposed to fluid shear stress, and the ATP concentration in the supernatant was determined at the indicated time points (see Figure 4E) using a bioluminescence assay (catalog A22066; Molecular Probes, Life Technologies) according to the manufacturer's instructions. Luminescence intensity was measured with a FlexStation 3 (Molecular Devices). ATP amounts were calculated with a calibration curve constructed using ATP standards. Parallel determination of lactate dehydrogenase (LDH) activity (catalog 10008882; Cayman Chemical) showed no LDH activity, excluding that cell damage contributed to the increased ATP release under fluid shear stress.

Animal models. All mice were backcrossed onto a C57BL/6N background at least 8 to 10 times, and experiments were performed with littermates as controls. Male and female animals (8–12 weeks old) were used unless stated otherwise. Mice were housed under a 12-hour light/12-hour dark cycle, with free access to food and water and under specific pathogen–free conditions unless stated otherwise. The generation of inducible endothelium-specific $G\alpha_q/G\alpha_{11}$-deficient mice (*Tie2-CreER^{T2} Gnaq$^{fl/fl}$ Gna11$^{-/-}$* [EC-q/11–KO]) was described previously (31). The generation of mice with inducible endothelium-specific deficiency of $P2Y_2$ (*Tie2-CreER^{T2} P2ry2$^{fl/fl}$* [EC-$P2Y_2$–KO]) is described in Supplemental Figure 5.

Telemetric blood pressure measurements. Measurements were performed in conscious, unrestrained mice with a radiotelemetry system (PA-C10; Data Sciences International) as described previously (49). Mice were caged with blinded identity and in random order.

Determination of nitrate and nitrite levels. Nitrate and nitrite (NOx) levels in plasma were measured with a highly sensitive HPLC system (ENO-20; Eicom) as described previously (50). Blood was collected from the retro-orbital sinus and immediately centrifuged at 6,800 *g* for 5 minutes at 4°C. Five days before the experiments commenced and throughout the observation period, animals were put on a standard chow diet (Lantmännen, Sweden) specifically selected for its low NOx content. Mice were caged with blinded identity and in random order. Flow-induced NOx release from endothelial cells in vitro was measured using a nitrate/nitrite fluorometric assay kit from Cayman Chemical according to the manufacturer's instructions.

Pressure myography. Animals were sacrificed, and the mesenteric arterial bed was removed and placed in ice-cold Krebs buffer (118.1 mM NaCl, 4.8 mM KCl, 2.5 mM $CaCl_2$, 1.2 mM $MgSO_4$, 1.2 mM KH_2PO_4, 25 mM $NaHCO_3$, 9.3 mM glucose, and 0.026 mM EDTA, pH 7.4, supplemented with 1% BSA). Arteries of the third or fourth branch were removed from the mesentery by gently peeling away the adventitia and were mounted in the proper proximal-distal orientation between 2 glass micropipettes seated in a chamber (Danish Myo Technology A/S). The inflow cannula was fixed, while the outflow cannula allowed for length adjustment along the longitudinal axis. The artery was secured on both ends by a 10.0 nylon suture and perfused with low-flow (5 μl/min) to remove any blood from the vessel lumen. The external diameter of the artery was visualized and recorded with a CCD camera using MyoVIEW software (Danish Myo Technology A/S). The temperature of the chamber was kept at a constant 37°C. The mounted artery was initially pressurized to 20 mmHg under no-flow conditions and incubated for 30 to 40 minutes. Pressure was then increased to 70 mmHg and the vessel was incubated for 10 minutes to allow it to reach a steady-state diameter. Vessels were contracted with 50 to 150 nM U46619 to 40% to 50% of the passive diameter. After reaching a stable baseline, flow was increased in a stepwise manner by changing the pressure of the inflow and outflow sides inversely, thereby creating a pressure difference across the arteriole without altering the intraluminal pressure. The viability of the vessel was verified at the end of the experiment by dilating the vessel with ACh (10 μM) or SNP (100 μM). Arteries showing less than 60% relaxation were considered damaged and were omitted from further analysis. Vasodilatation to flow was calculated as a percentage of the U46619-induced contraction as described previously (51) by the following equation: percentage of relaxation = $100 \times (D_F - D_{U46619})/(D_{PD} - D_{U46619})$, where D represents the external diameter of the vessels; D_F is the vessel diameter during flow; D_{U46619} is the diameter after U46619 contraction; and D_{PD} is the passive diameter without any treatment. Mice used for the experiments were caged with blinded identity and in random order.

Expression analysis. RNA isolation and transcription were performed as described previously (48). Primers were designed with the online tool provided by Roche, and quantification was performed using the LightCycler 480 Probe Master System (Roche). Genomic DNA was used as a universal standard to calculate the gene copy number per nanogram of RNA. Relative expression levels were obtained by normalization with *GAPDH* or 18S values.

qPCR primer sequences. The qPCR primer sequences were as follows: *GNAQ* (human) forward: 5′-GACTACTTCCCAGAATATGATGGAC-3′, reverse: 5′-GGTTCAGGTCCACGAACATC-3′; *GNA11* (human) forward: 5′-GCATCCAGGAATGCTACGAC-3′, reverse: 5′-GGTCAACGTCGGTCAGGTAG-3′; *Gnaq* (mouse) forward: 5′-GACTACTTCCCAGAATATGATGGAC-3′, reverse: 5′-TCAGGATGAATTCTCGAGCTG-3′; *Gna11* (mouse) forward: 5′-CACTGGCATCATCGAGTACC-3′, reverse: 5′-GATCCACTTCCTGCGCTCT-3′; *Gnaq* (bovine) forward: 5′-TGGGTCGGGCTACTCTGAT-3′, reverse: 5′-TAGGGGATCTTGAGCGTGTC-3′; *Gna11* (bovine) forward: 5′-GAGCACGTTCATCAAGCAGA-3′, reverse: 5′-GATGTTCTGGTACACCAGTTTGG-3′; *GAPDH* (human) forward: 5′-GCATCCTGGGCTACACTGA-3′, reverse: 5′-CCAGCGTCAAAGGTGGAG-3′; *GAPDH* (mouse) forward: 5′-AGCTTGTCATCAACGGGAAG-3′, reverse: 5′-TTTGATGTTAGTGGGGTCTCG-3′; *GAPDH* (bovine) forward: 5′-TCACCAGGGCTGCTTTTAAT-3′, reverse: 5′-GAAGGTCAATGAAGGGGTCA-3′; *P2YR2* (human) forward: 5′-TAACCTGCCACGACACCTC-3′, reverse: 5′-CTGAGCTGTAGGCCACGAA-3′; *P2yr2* (mouse) forward: 5′-TGGTACTGGCCGTCTTCG-3′, reverse: 5′-AGTAGAGGGTGCGCGTGA-3′; *P2yr2* (bovine) forward: 5′-AGAACTCCAGGGGGACAGA-3′, reverse: 5′-CAGCCAGATGTCCTTAGTGTCA-3′; *P2XR4* (human) forward: 5′-AGCCCCATCAAAGAACAGAG-3′, reverse: 5′-TCTCTGGGGTGATGTGGTG-3′; 18S (mouse) forward: 5′-GCAATTATTCCCCATGA-3′, reverse: 5′-GGGACTTAATCAACGCAAGC-3′; *Cdh5* (VE-cadherin; mouse) forward: 5′-CCATGATCGACGTGAAGAAA-3′, reverse: 5′-GATGTGCAGTGTGTCGTATGG-3′; and β-actin (mouse) forward: 5′-AAATCGTGCGTGACATCAAA-3′, reverse: 5′-TCTCCAGGGAGGAAGAGGAT-3′.

Statistics. Trial experiments or experiments performed previously were used to determine sample size with adequate statistical power. Samples were excluded in cases in which RNA and cDNA quality or

tissue quality after processing was poor (below commonly accepted standards). Data are presented as the mean ± SEM. Comparisons between 2 groups were performed with an unpaired 2-tailed Student's *t* test, and multiple group comparisons at different time points were performed by 2-way ANOVA, followed by Bonferroni's post-hoc test. A *P* value of 0.05 or less was considered statistically significant.

Study approval. All procedures involving animal care and use in this study were approved by the local animal ethics committees (Regierungspräsidia Karlsruhe and Darmstadt, Germany).

Acknowledgments

We thank Sharon Meaney-Gardian and Svea Hümmer for their secretarial help. This work was supported by the Collaborative Research Center 834 of the German Research Foundation.

Address correspondence to: Stefan Offermanns, Max Planck Institute for Heart and Lung Research, Ludwigstrasse 43, 61231 Bad Nauheim, Germany. Phone: 49.0.6032.705.1201; E-mail: stefan.offermanns@mpi-bn.mpg.de.

1. Lawes CM, Vander Hoorn S, Rodgers A. Global burden of blood-pressure-related disease, 2001. *Lancet*. 2008;371(9623):1513–1518.
2. Kearney PM, Whelton M, Reynolds K, Muntner P, Whelton PK, He J. Global burden of hypertension: analysis of worldwide data. *Lancet*. 2005;365(9455):217–223.
3. Davies PF. Flow-mediated endothelial mechanotransduction. *Physiol Rev*. 1995;75(3):519–560.
4. Feletou M, Kohler R, Vanhoutte PM. Endothelium-derived vasoactive factors and hypertension: possible roles in pathogenesis and as treatment targets. *Curr Hypertens Rep*. 2010;12(4):267–275.
5. Busse R, Fleming I. Regulation of endothelium-derived vasoactive autacoid production by hemodynamic forces. *Trends Pharmacol Sci*. 2003;24(1):24–29.
6. Fleming I. Molecular mechanisms underlying the activation of eNOS. *Pflugers Arch*. 2010;459(6):793–806.
7. Dimmeler S, Fleming I, Fisslthaler B, Hermann C, Busse R, Zeiher AM. Activation of nitric oxide synthase in endothelial cells by Akt-dependent phosphorylation. *Nature*. 1999;399(6736):601–605.
8. Fulton D, et al. Regulation of endothelium-derived nitric oxide production by the protein kinase Akt. *Nature*. 1999;399(6736):597–601.
9. Balligand JL, Feron O, Dessy C. eNOS activation by physical forces: from short-term regulation of contraction to chronic remodeling of cardiovascular tissues. *Physiol Rev*. 2009;89(2):481–534.
10. Bagi Z, Frangos JA, Yeh JC, White CR, Kaley G, Koller A. PECAM-1 mediates NO-dependent dilation of arterioles to high temporal gradients of shear stress. *Arterioscler Thromb Vasc Biol*. 2005;25(8):1590–1595.
11. Liu Y, Bubolz AH, Shi Y, Newman PJ, Newman DK, Gutterman DD. Peroxynitrite reduces the endothelium-derived hyperpolarizing factor component of coronary flow-mediated dilation in PECAM-1-knockout mice. *Am J Physiol Regul Integr Comp Physiol*. 2006;290(1):R57–R65.
12. Fleming I, Fisslthaler B, Dixit M, Busse R. Role of PECAM-1 in the shear-stress-induced activation of Akt and the endothelial nitric oxide synthase (eNOS) in endothelial cells. *J Cell Sci*. 2005;118(pt 18):4103–4111.
13. Tzima E, et al. A mechanosensory complex that mediates the endothelial cell response to fluid shear stress. *Nature*. 2005;437(7057):426–431.
14. Goel R, et al. Site-specific effects of PECAM-1 on atherosclerosis in LDL receptor-deficient mice. *Arterioscler Thromb Vasc Biol*. 2008;28(11):1996–2002.
15. Harry BL, et al. Endothelial cell PECAM-1 promotes atherosclerotic lesions in areas of disturbed flow in ApoE-deficient mice. *Arterioscler Thromb Vasc Biol*. 2008;28(11):2003–2008.
16. Conway D, Schwartz MA. Lessons from the endothelial junctional mechanosensory complex. *F1000 Biol Rep*. 2012;4:1.
17. Conway DE, Breckenridge MT, Hinde E, Gratton E, Chen CS, Schwartz MA. Fluid shear stress on endothelial cells modulates mechanical tension across VE-cadherin and PECAM-1. *Curr Biol*. 2013;23(11):1024–1030.
18. Hur SS, et al. Roles of cell confluency and fluid shear in 3-dimensional intracellular forces in endothelial cells. *Proc Natl Acad Sci U S A*. 2012;109(28):11110–11115.
19. Barakat AI, Lieu DK, Gojova A. Secrets of the code: do vascular endothelial cells use ion channels to decipher complex flow signals? *Biomaterials*. 2006;27(5):671–678.
20. Li J, et al. Piezo1 integration of vascular architecture with physiological force. *Nature*. 2014;515(7526):279–282.
21. Ranade SS, et al. Piezo1, a mechanically activated ion channel, is required for vascular development in mice. *Proc Natl Acad Sci U S A*. 2014;111(28):10347–10352.
22. Weinbaum S, Tarbell JM, Damiano ER. The structure and function of the endothelial glycocalyx layer. *Annu Rev Biomed Eng*. 2007;9:121–167.
23. Tarbell JM, Simon SI, Curry FR. Mechanosensing at the vascular interface. *Annu Rev Biomed Eng*. 2014;16:505–532.
24. Egorova AD, van der Heiden K, Poelmann RE, Hierck BP. Primary cilia as biomechanical sensors in regulating endothelial function. *Differentiation*. 2012;83(2):S56–S61.
25. Kuchan MJ, Jo H, Frangos JA. Role of G proteins in shear stress-mediated nitric oxide production by endothelial cells. *Am J Physiol*. 1994; 267(3 pt 1):C753–C758.
26. Jo H, Sipos K, Go YM, Law R, Rong J, McDonald JM. Differential effect of shear stress on extracellular signal-regulated kinase and N-terminal Jun kinase in endothelial cells. Gi2- and Gβ/γ-dependent signaling pathways. *J Biol Chem*. 1997;272(2):1395–1401.
27. Otte LA, et al. Rapid changes in shear stress induce dissociation of a G alpha(q/11)-platelet endothelial cell adhesion molecule-1 complex. *J Physiol*. 2009;587(pt 10):2365–2373.
28. Melchior B, Frangos JA. Distinctive subcellular akt-1 responses to shear stress in endothelial cells. *J Cell Biochem*. 2014;115(1):121–129.
29. Hahn C, Schwartz MA. Mechanotransduction in vascular physiology and atherogenesis. *Nat Rev Mol Cell Biol*. 2009;10(1):53–62.
30. Tarbell JM, Shi DF, Dunn J, Jo H. Fluid mechanics, arterial disease and gene expression. *Annu Rev Fluid Mech*. 2014;46:591–614.
31. Korhonen H, et al. Anaphylactic shock depends on endothelial Gq/G11. *J Exp Med*. 2009;206(2):411–420.
32. Gericke A, et al. Role of M1, M3, and M5 muscarinic acetylcholine receptors in cholinergic dilation of small arteries studied with gene-targeted mice. *Am J Physiol Heart Circ Physiol*. 2011;300(5):H1602–H1608.
33. Rudic RD, Shesely EG, Maeda N, Smithies O, Segal SS, Sessa WC. Direct evidence for the importance of endothelium-derived nitric oxide in vascular remodeling. *J Clin Invest*. 1998;101(4):731–736.
34. Yamamoto K, et al. Impaired flow-dependent control of vascular tone and remodeling in P2X4-deficient mice. *Nat Med*. 2006;12(1):133–137.
35. Abbracchio MP, et al. International Union of Pharmacology LVIII: update on the P2Y G protein-coupled nucleotide receptors: from molecular mechanisms and pathophysiology to therapy. *Pharmacol Rev*. 2006;58(3):281–341.
36. Burnstock G, Ralevic V. Purinergic signaling and blood vessels in health and disease. *Pharmacol Rev*. 2014;66(1):102–192.
37. Bodin P, Bailey D, Burnstock G. Increased flow-induced ATP release from isolated vascular endothelial cells but not smooth muscle cells. *Br J Pharmacol*. 1991;103(1):1203–1205.
38. Yamamoto K, Furuya K, Nakamura M, Kobatake E, Sokabe M, Ando J. Visualization of flow-induced ATP release and triggering of Ca^{2+} waves at caveolae in vascular endothelial cells. *J Cell Sci*. 2011;124(pt 20):3477–3483.
39. John K, Barakat AI. Modulation of ATP/ADP concentration at the endothelial surface by shear stress: effect of flow-induced ATP release. *Ann Biomed Eng*. 2001;29(9):740–751.
40. Storch U, Mederos y Schnitzler M, Gudermann T. G protein-mediated stretch reception. *Am J Physiol Heart Circ Physiol*. 2012;302(6):H1241–H1249.
41. Chachisvilis M, Zhang YL, Frangos JA. G protein-coupled receptors sense fluid shear stress in endothelial cells. *Proc Natl Acad Sci U S A*. 2006;103(42):15463–15468.
42. Jung B, et al. Flow-regulated endothelial S1P receptor-1 signaling sustains vascular development. *Dev Cell*. 2012;23(3):600–610.
43. Chun J, Hla T, Lynch KR, Spiegel S, Moolenaar WH. International Union of Basic and Clinical Pharmacology. LXXVIII. Lysophospho-

lipid receptor nomenclature. *Pharmacol Rev*. 2010;62(4):579–587.
44. Yamamoto K, Sokabe T, Ohura N, Nakatsuka H, Kamiya A, Ando J. Endogenously released ATP mediates shear stress-induced Ca2+ influx into pulmonary artery endothelial cells. *Am J Physiol Heart Circ Physiol*. 2003;285(2):H793–H803.
45. Lohman AW, Billaud M, Isakson BE. Mechanisms of ATP release and signalling in the blood vessel wall. *Cardiovasc Res*. 2012;95(3):269–280.
46. Yamamoto K, Korenaga R, Kamiya A, Qi Z, Sokabe M, Ando J. P2X(4) receptors mediate ATP-induced calcium influx in human vascular endothelial cells. *Am J Physiol Heart Circ Physiol*. 2000;279(1):H285–H292.
47. Raqeeb A, Sheng J, Ao N, Braun AP. Purinergic P2Y2 receptors mediate rapid Ca(2+) mobilization, membrane hyperpolarization and nitric oxide production in human vascular endothelial cells. *Cell Calcium*. 2011;49(4):240–248.
48. Sivaraj KK, Takefuji M, Schmidt I, Adams RH, Offermanns S, Wettschureck N. G13 controls angiogenesis through regulation of VEGFR-2 expression. *Dev Cell*. 2013;25(4):427–434.
49. Wirth A, et al. G12-G13-LARG-mediated signaling in vascular smooth muscle is required for salt-induced hypertension. *Nat Med*. 2008;14(1):64–68.
50. Jansson EA, et al. A mammalian functional nitrate reductase that regulates nitrite and nitric oxide homeostasis. *Nat Chem Biol*. 2008;4(7):411–417.
51. Liu C, et al. Depletion of intracellular Ca^{2+} stores enhances flow-induced vascular dilatation in rat small mesenteric artery. *Br J Pharmacol*. 2006;147(5):506–515.